Available online at www.sciencedirect.com
SCIENCE DIRECT®
Microporous and Mesoporous Materials 66 (2003) 37–51
MICROPOROUS AND MESOPOROUS MATERIALS
www.elsevier.com/locate/micromeso

# A method of synthesis of silicious inorganic ordered materials (MCM-41–SBA-1) employing polyacrylic acid–$C_n$TAB–TEOS nanoassemblies

C.C. Pantazis [a,*], P.N. Trikalitis [b], P.J. Pomonis [a], M.J. Hudson [c]

[a] *Department of Chemistry, University of Ioannina, Ioannina 45110, Greece*
[b] *Department of Chemistry, Michigan State University, East Lansing, MI 48824, USA*
[c] *School of Chemistry, University of Reading, Whiteknights, Reading RG6 6AD, UK*

Received 20 May 2003; received in revised form 6 August 2003; accepted 26 August 2003

**Abstract**

In this work we describe the synthesis of a variety of MCM-41 type hexagonal and SBA-1 type cubic mesostructures and mesoporous silicious materials employing a novel synthesis concept based on polyacrylic acid (Pac)–$C_n$TAB complexes as backbones of the developing structures. The ordered porosity of the solids was established by XRD and TEM techniques. The synthesis concept makes use of Pac–$C_n$TAB nanoassemblies as a preformed scaffold, formed by the gradual increase of pH. On this starting matrix the inorganic precursor species $SiO_2$ precipitate via hydrolysis of TEOS under the influence of increasing pH. The molecular weight (MW) of Pac, as well as the length of carbon chain in $C_n$TAB, determine the physical and structural characteristics of the obtained materials. Longer chain surfactants ($C_{16}$TAB) lead to the formation of hexagonal phase, while shorter chain surfactants ($C_{14}$TAB, $C_{12}$TAB) favor the SBA-1 phase. Lower MW of Pac (≈2000) leads to better-organized structures compared to higher MW (≈450,000), which leads to worm-like mesostructures. Cell parameters and pore size increase with increasing polyelectrolyte and/or surfactant chain, while at the same time SEM photography reveals that the particle size decreases. Conductivity experiments provide some insight into the proposed self-assembling pathway.


*Keywords:* Hybrid materials; Polyacrylic acid–surfactant complexes; Mesoporous materials; Self-organized systems

## 1. Introduction

Silica-based mesoporous materials are synthesized by cooperative assembly of periodic inorganic and surfactant-based structures. The process is governed by the matching of charge density at the surfactant/inorganic interface. Added to the original path ($S^+I^-$) [1], other pathways of self-assembly leading to ordered mesostructures have also been proposed by Stucky and co-workers, namely ($S^-I^+$), ($S^+X^-I^+$) and ($S^-M^+I^-$) [2], where S, X, M, I correspond to surfactant, halide, cation, and inorganic species respectively. Moreover non-ionic diblock and/or triblock copolymers, have been successfully used as structure directing agents

* Corresponding author. Tel.: +32-651098361; fax: +32-651098795.
*E-mail address:* me00596@cc.uoi.gr (C.C. Pantazis).

1387-1811/$ - see front matter © 2003 Published by Elsevier Inc.
doi:10.1016/j.micromeso.2003.08.017

for the preparation of ordered mesoporous silica [3]. The self-organization process of the latter is expected to be fulfilled through an intermediate of the form ($S^0H^+X^-I^+$).

Other systems known to generate mesoporous silica, of lower degree of ordering or disordered wormhole structures, include the use of cationic and anionic block copolymers [4] or non-ionic surfactants in aqueous solutions [5]. The above systems offer valuable knowledge and a span of workable methods of manipulating the mesoscopic regime in nanodimensions.

The characteristic feature of modular chemistry is the prefabrication of the structural components, which combine together and then self-assemble into a well organized superstructure obeying principles of hierarchical construction. In such a way it is possible to generate multifunctional materials [6–8], whose properties can be synergistic or a combination of those of the initial subunits. Furthermore novel properties can emerge from the built-up of matter on different scales. By observing similar systems in Nature, various researchers have developed biomimetic approaches for mineralization in order to understand the basic underlying principles of supramolecular chemistry. Thus Ozin and co-workers have developed biomimetically mineralized aluminiphosphate-based ultrastructures using micellar, lamellar and vesicular templates, which account for order on the mesoscopic and microscopic or macroscopic length scales respectively [9]. Mann and co-workers on the other hand have used self-organized microemulsions as templates to produce cellular type films of calcium carbonate on planar and spherical substrates [10].

In the context of this work, we have investigated another type of template as a preorganized scaffold in a hybrid organic/inorganic ordered nanoassembly, namely polyelectrolyte–surfactant complexes. Such complexes are known for quite a long time as a new type of highly ordered mesomorphous *organic* solids [11–13]. The most interesting candidate is the group of polyacrylic acid–$C_n$TAB (Pac$C_n$) complexes studied by Antonietti and Conrad. These researchers established a fcc symmetry type for the Pac250$C_{12}$ organic assembly (Pac250 stands for polyacrylic acid of MW = 250,000 g mol$^{-1}$) resulting from properly packed cylinders [11]. The formation of the complex follows a highly cooperative zipper mechanism under a stoichiometry of 1:1, driven by coulombic interactions between the functional groups of the anionic polyelectrolyte backbone and the cationic surfactant as well as hydrophobic interactions among the surfactant chains, whilst the ordered phase arouses from the amphotropy of the system, i.e. the incompatibility between the ionic backbone and the alkyl chains. The whole process is governed by neighboring group effects even at very low surfactant concentration, the linear charge density of the polyelectrolyte and the presence of other cations [14]. However, to our knowledge, no work has been so far reported in the open literature on the possible potential of these type of solids towards the nanodesign of hybrid organic/inorganic mesostructures and the eventual development of ordered mesoporous inorganic materials. In this work we report the mechanism of development and the main features of organized silicious mesostuctures developed via Pac–$C_n$TAB precursors and the use of TEOS as a source of silica.

## 2. Experimental

### 2.1. Synthesis protocol

At ambient temperature 0.5 g of polyacrylic acid, or its sodium salt, (Aldrich) of the desired MW (2000–450,000 a.u.) was dissolved in 100 g of water under stirring. The pH of the solution, measured online, was typically pH $\approx$ 3.2. HCl acid is then used to set pH at 1.5. Then $C_{14}$TAB or $C_{16}$TAB (Merck) is added at a stoichiometric amount with respect to polyelecrolyte functional groups (e.g. 2.5 g of $C_{16}$TAB are needed for use with Pac of MW = 2000 a.u.). After this addition a clear solution was obtained. Finally, 5 ml TEOS (Merck) was introduced into the Pac–$C_n$TAB. Then a slow dropwise addition of $NH_3$ started taking place for about 2 h. Intermediate samples were isolated at any desired pH, which was followed and recorded via a pHmeter during the process. The process of increase of pH leads eventually to precipitation of a white solid. Pre-

cipitates at a final pH 5.5, were left for 24 h in the mixture, unless stated otherwise. The samples are then subject to filtration, washing with water, drying at 90 °C ($T_g = 106$ °C for polyacrylic acid) and calcination at 600 °C for 6 h with a heating rate 2 °C min$^{-1}$ under atmospheric conditions.

### 2.2. Instrumentation and characterization

Nitrogen adsorption measurements were performed at 77 K on a Sorptomatic 9000 Fisons Instrument after outgassing for 12 h at 473 K and $P = 5 \times 10^{-3}$ Torr. X-ray diffraction measurements were acquired on a Bruker Advance D8 system using CuK$\alpha$ radiation ($\lambda = 1.5418$ Å) with a resolution of 0.01°. Scanning electron microscopy (SEM) was performed on a Jeol JSM 5600 at 20 kV. TEM photos were recordered in a JEOL 120CX instrument equipped with CeB6 filament. Simultaneous TG/DSC analysis were carried out on a Netzsch Thermoanalyzer STA 449 C in air with a heating rate of 10 K/min. Finally, simultaneous pH and conductivity measurements were performed on an Inolab Terminal 3 by WTW.

## 3. Results

The system Pac/$C_n$TAB/TEOS/W can generate a number of different materials by applying the synthesis protocol mentioned above and varying the MW of polyacrylic acid (Pac), the chain length ($n$) in $C_n$TAB as well as the pH at which the samples are isolated. In Table 1 there are such typical samples together with some of their properties.All the samples in this table, as well as in the following discussion, were developed from the components Pac$X$/$C_n$TAB/TEOS/W, where $n$—the number of carbon atoms constituting the aliphatic chain and takes values $n = 12$, 14 or 16 in this work and $X$ corresponds to the MW of Pac$\times 10^3$. In other words $X = 2$ means MW = 2000, $X = 450$ means MW = 450,000 etc. In cases where not the pure acid, but the sodium (Na) salt of Pac was used, there is the corresponding designation. For shortening the designation will be Pac$X$C$_n$.

In Fig. 1 there are some TEM images of samples included in Table 1.

All samples in Fig. 1 have been prepared using $C_{16}$TAB and Pac with varying MW. It is clear that the samples exhibit a hexagonal structure, which is better organized in the samples obtained using Pac of low MW (2000–15,000) as compared to samples employing Pac of high MW (250,000–450,000). This effect should be due to the unfolding of the polymer chains [15], which is more favorable in the first case, resulting in better-organized structures. The structure of Pac should change upon complexaton with the surfactant. We should expect for Pac of low MW 2000 a.u. to be almost linear. The

Table 1
Structural, surface and pore characteristics of the corresponding samples[a]

| Sample code | Phase (XRD) | Ssa/BET ($m^2 g^{-1}$) | Pore volume ($cm^3 g^{-1}$) | $a_0$[b] (nm) | $a_0$[c] (nm) | Horvath–Kawazoe pore diameter $d_{max}$ (nm) | Wall thickness $w$ (nm) ($w = a_0^3 - d_{max}$) |
|---|---|---|---|---|---|---|---|
| Pac2C$_{16}$ | Hexagonal (MCM-41) | 1285 | 0.89 | 4.5 | 3.7 | 2.3 | 1.4 |
| Pac15(Na)C$_{16}$ | Hexagonal (MCM-41) | 1113 | 0.73 | 4.6 | 3.6 | 2.3 | 1.3 |
| Pac250C$_{16}$ | Hexagonal (MCM-41) | 1300 | 1.0 | 4.7 | 4.2 | 2.9 | 1.3 |
| Pac450C$_{16}$ | Disord. hexagonal—worm-like | 933 | 1.1 | 4.8 | 4.6 | 2.9 | 1.7 |
| Pac2C$_{14}$ | Cubic SBA-1 | 1300 | 0.78 | 8.2 | 7.2 | 2.2 | – |
| Pac15(Na)C$_{14}$ | Cubic SBA-1 | – | – | 8.4 | – | – | – |
| Pac2C$_{12}$ | Cubic SBA-1 | 1283 | 0.87 | 7.4 | 6.9 | 1.8 | – |

[a] Pac$X$—polyacrylic acid of MW = $X \cdot 10^3$. (Na) Polyacrylic sodium salt was used, $n$ in $C_n$TAB—the number of carbon atoms in the surfactant chain.

[b] Refers to the uncalcined samples and calculated as $a_0 = 2d_{100}/3^{1/2}$ for the hexagonal phase and $a_0 = d_{hkl} * (h^2 + k^2 + l^2)^{1/2}$ for the cubic phase.

[c] Refers to the calcined at 600 °C samples.

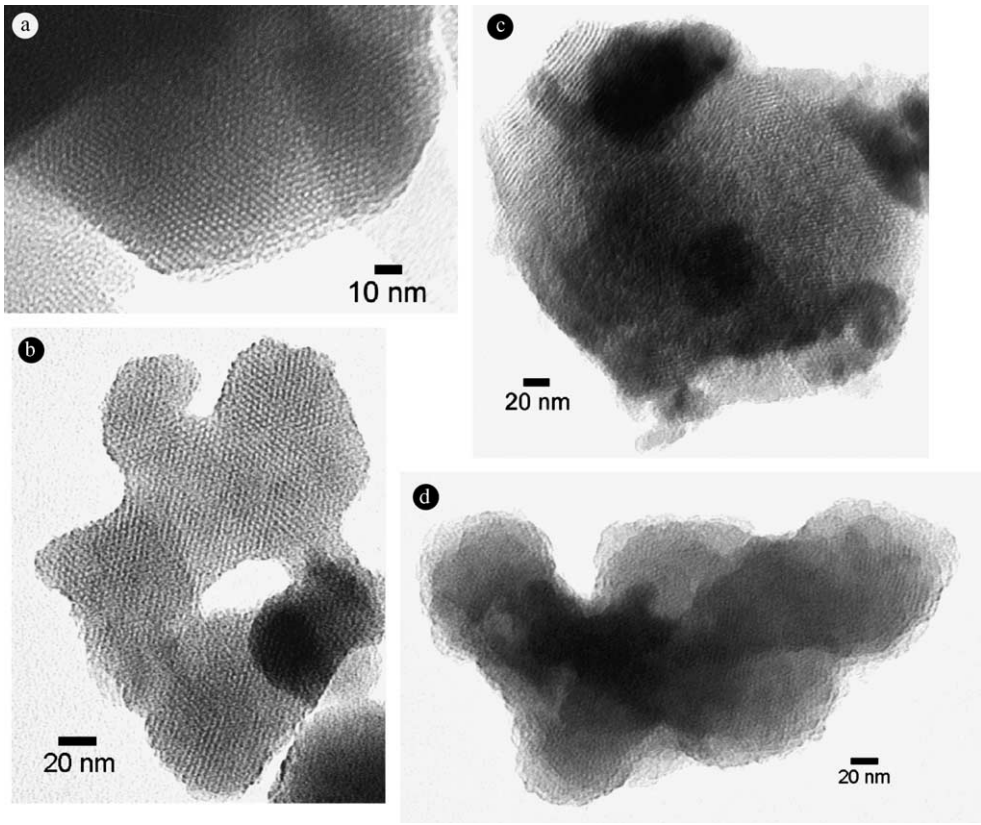


Fig. 1. TEM micrographs of (a) Pac2$C_{16}$, (b) Pac15(Na)$C_{16}$, (c) Pac250$C_{16}$ and (d) Pac450$C_{16}$ calcined at 600 °C mesoporous silica. All samples, developed with $C_{16}$TAB, exhibit hexagonal pore order, which is better organized and more clear in the cases of Pac of lower MW, i.e. 2000 (a) and 15,000 (b).

chain of Pac of very large MW 250,000 or 450,000 should tend to fold. However as complexed to the surfactant probably they become more linear and organized. But as pH is <7 not 100% complexation has taken place and the uncomplexed folded Pac chain is probably responsible for the introduction of disorder in the mesophase.

For the materials developed using $C_{12}$TAB and $C_{14}$TAB, it was not possible to obtain TEM images since the materials proved very sensitive and were destroyed under the electron beam. In Fig. 2 the SEM photographs of the same samples are shown in the same magnification ×20,000, except for Pac450$C_{16}$, which is ×30,000. It is clearly observed (Fig. 2) that as MW of Pac increases (2000 → 15,000 → 250,000 → 450,000), the particle size decreases gradually from an average of 1 μm for Pac2$C_{16}$ to around 100–200 nm for Pac450$C_{16}$. This effect might be related to better crystallization conditions in the former case as compared to inferior crystallization conditions in the second. It is worthnoticing that the Pac2$C_{16}$ structure, which posseses the best hexagonal ordering in TEM (Fig. 1) shows also for the uncalcined sample (inset in Fig. 2) some hexagonal flake-like crystallites with diameter $l \approx 0.1$ μm.

In Fig. 3 the XRD results for the samples Pac$XC_n$ ($X = 2$, 15(Na), 250 and 450) are presented.

Shown in Fig. 3 are the X-ray powder diffraction pattern of Pac2$C_{16}$, Pac15(Na)$C_{16}$, Pac250$C_{16}$ and Pac450$C_{16}$. The uncalcined samples Pac2$C_{16}$, Pac15(Na)$C_{16}$, Pac250$C_{16}$ show three to four well defined Bragg peaks in the low angle region

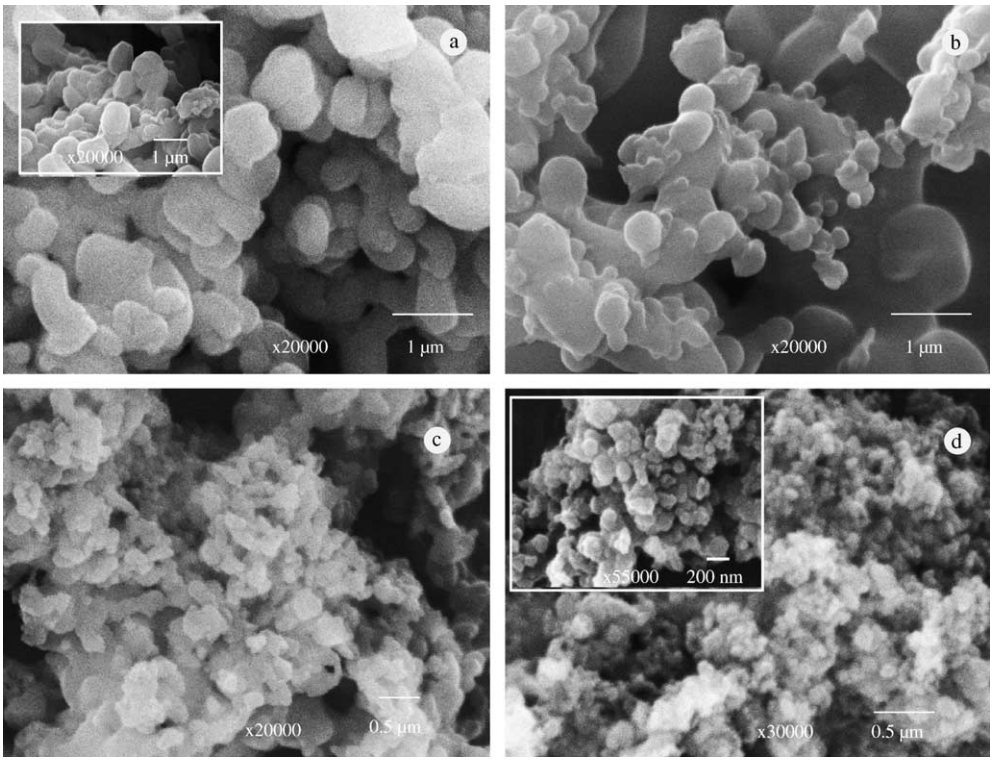


Fig. 2. SEM micrographs of (a) Pac2$C_{16}$, (b) Pac15(Na)$C_{16}$, (c) Pac250$C_{16}$ and (d) Pac450$C_{16}$ calcined samples revealing the decreasing particle size in this sequence. Inset in (a) shows the uncalcined Pac2$C_{16}$ sample exhibiting a plate-like hexagonal particle morphology of 1 μm size. Inset in (d) shows magnified particles of size 100–200 nm of Pac450$C_{16}$ calcined sample.

$2° < 2\theta < 7°$, fully indexed to a hexagonal unit cell. These patterns are typical of hexagonal mesostructured MCM-41 type materials. For Pac450$C_{16}$ only one low angle peak is observed, characteristic of worm-like mesostructured solid. The high order reflections (1 1 0) and (2 0 0) are not well resolved in the XRD pattern of the corresponding calcined samples, suggesting a decrease of the long-range hexagonal order. Moreover, the template-free materials show a small contraction of the unit cell as indicated by the shift at higher angles of the (1 0 0) reflection.

In Fig. 4 the XRD data for the Pac2$C_{12}$, Pac2$C_{14}$ and Pac15(Na)$C_{14}$, are shown. The uncalcined samples show three low angle Bragg peaks that are fully indexed to cubic unit cell (see Table 1). These XRD patterns are typical of cubic SBA-1 type mesostructured materials [16]. The XRD patterns of the calcined materials show that the cubic pore order is retained, however the coherence length is smaller, as indicated by the broader Bragg reflections. Note, however that the heated at 600 °C sample Pac15(Na)$C_{14}$, shows a collapsed pore structure. This fact probably indicates, as explained in the discussion, that the SBA-1 structure is more sensitive to heating in the presence of Na-cations and/or longer polyelectrolyte chains than the hexagonal Pac15(Na)$C_{16}$. That is also the reason we did not proceed to produce the SBA-1 phase using Pac of even higher MW.

In the same Fig. 4, top left graph, the XRD pattern of an uncalcined sample isolated at pH 4 is shown for the Pac2$C_{12}$ sample ($a_1$). We observe that the same cubic structure is formed and detected already at this low pH, slightly above the

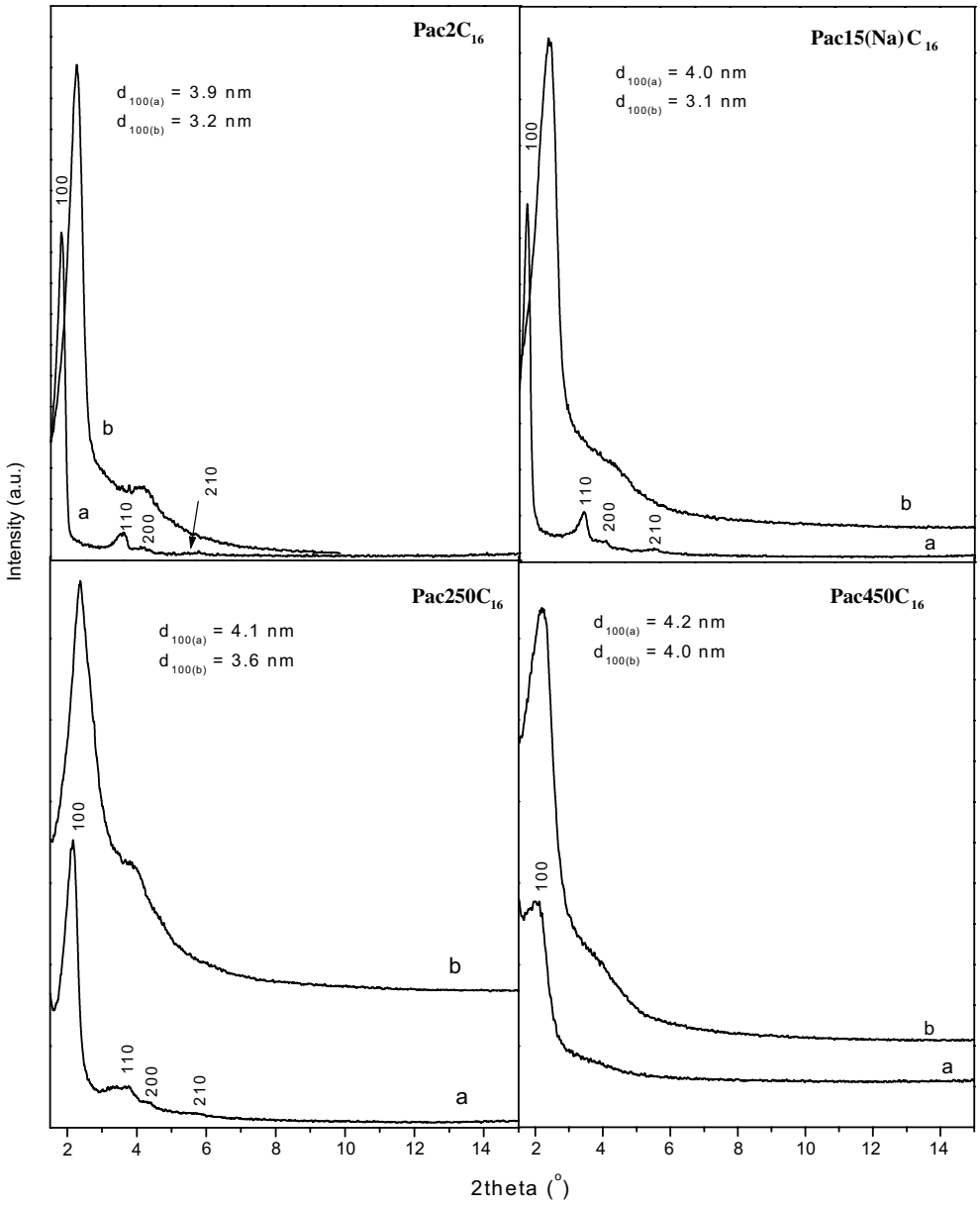


Fig. 3. X-ray diffractograms of (a) uncalcined (dried at 90 °C) and (b) calcined at 600 °C Pac$XC_n$ samples indicated. All samples developed with $C_{16}$TAB, exhibit characteristic MCM-41 patterns.

pH $\approx$ 3.3 where the precipitates first appear, implying that the system does not undergo any phase transitions, but the corresponding cell parameter $a_0 = 7.1$ nm is lower compared to the structure isolated at pH $\approx$ 5, where $a_0 = 7.4$.

These results clearly show that for the same polyelectrolyte chain length, the use of $C_n$TAB ($n = 12,14$) favors cubic SBA-1 mesoporous materials while the longer chain surfactant $C_{16}$TAB leads to hexagonal MCM-41 type solids.

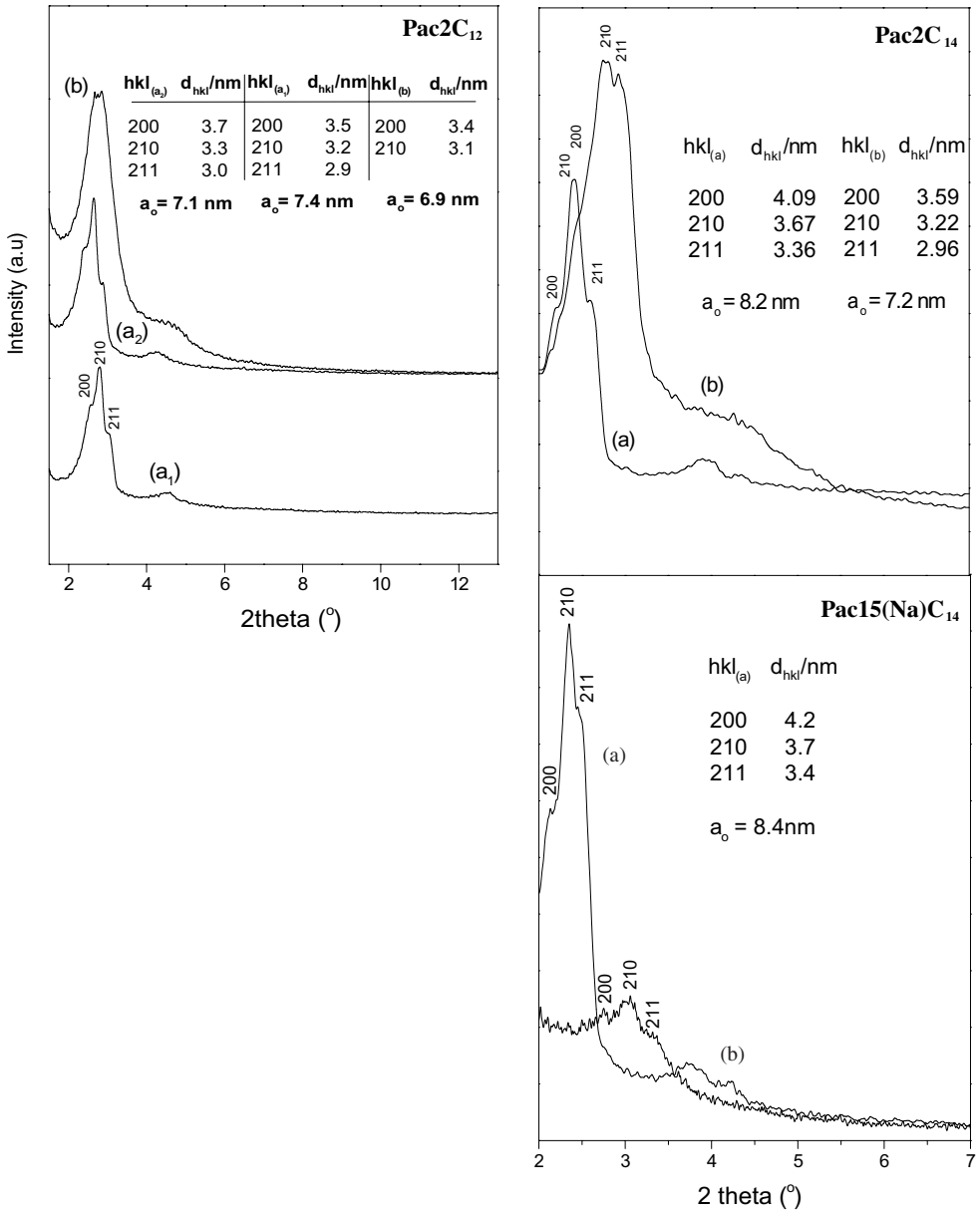


Fig. 4. X-ray diffractograms of (a) uncalcined (dried at 90 °C) and (b) calcined at 600 °C Pac$XC_n$ samples indicated. In Pac2$C_{12}$ ($a_1$) corresponds to the uncalcined intermediate sample isolated at pH 4, ($a_2$) to the uncalcined intermediate sample isolated at pH 5.5 and (b) the calcined ($a_2$). Notice that these samples developed with $C_{12}$TAB and $C_{14}$TAB exhibit cubic SBA-1 patterns in contrast to the samples in Fig. 3, where the use of $C_{16}$TAB leads to MCM-41 type patterns.

In Fig. 5 typical $N_2$ adsorption–desorption isotherms (77 K) are shown. The pore size distributions in the same figure have been calculated according to the Horvath–Kawazoe method. The four diagrams in the upper part of this Fig. 5 belong to the samples synthesized using $C_{16}$TAB and

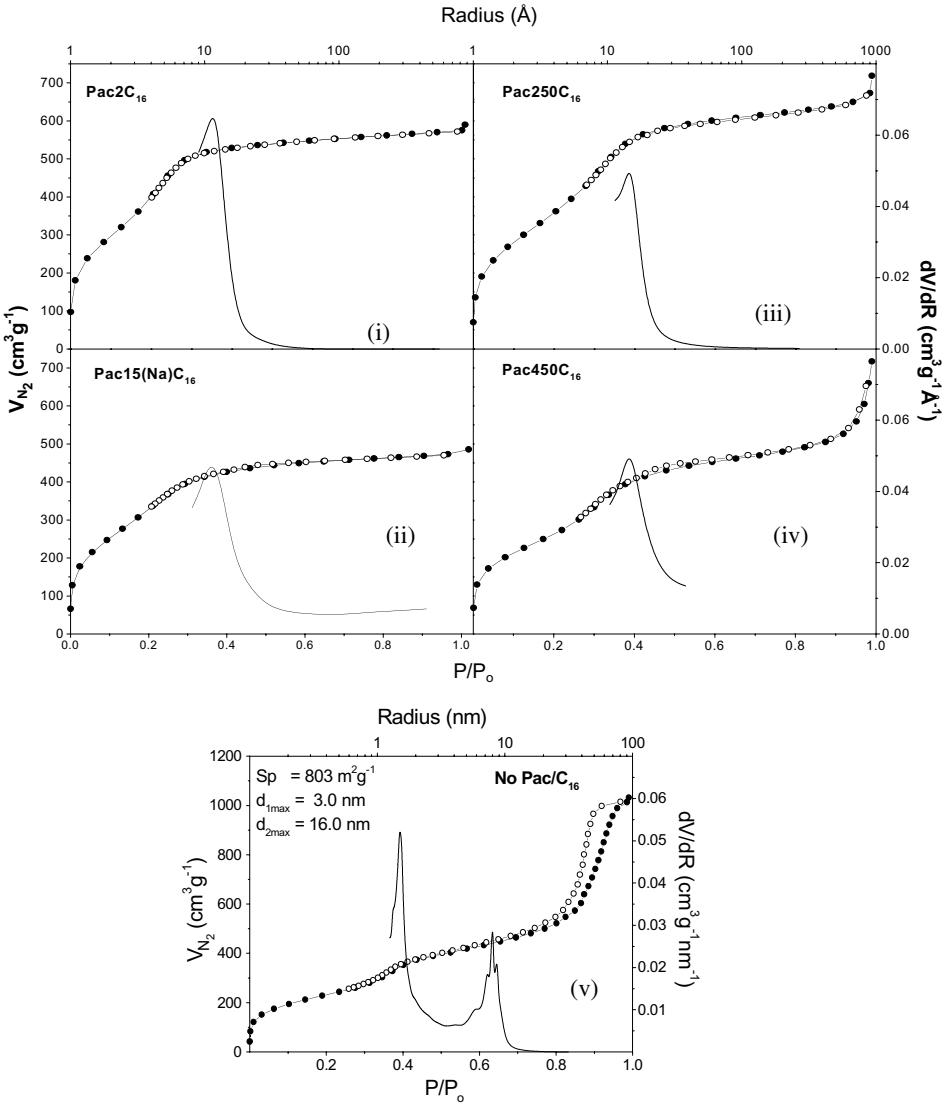


Fig. 5. $N_2$ adsorption–desorption isotherms (77 K) for the indicated solids. The pore size distributions have been calculated according to the Horvath–Kawazoe method and are summarized in Table 1. The four samples in upper part correspond to the ones in Fig. 3 and exhibit hexagonal MCM-41 structure. The two samples in the lower part correspond to the ones in Fig. 4 and exhibit cubic SBA-1 structure. The sample in the middle was developed without the addition of Pac. Clearly Pac molecules act as organizers of the mesostructure.

Pac with different MW's plus TEOS. The two diagrams in the lower part correspond to the samples synthesized using $C_{12}$TAB or $C_{14}$TAB and Pac with MW = 2000. Finally, the diagram in the middle corresponds to the sample prepared using $C_{16}$TAB plus TEOS, but without Pac.

In the low relative pressure region the Pac$XC_{16}$ materials exhibit a steeper condensation step as we move from Pac450$C_{16}$ → Pac250$C_{16}$ → Pac2$C_{16}$, indicating more uniform pore channels, while Pac15(Na)$C_{16}$ shows a more smooth condensation step indicating a degree of structural collapse.

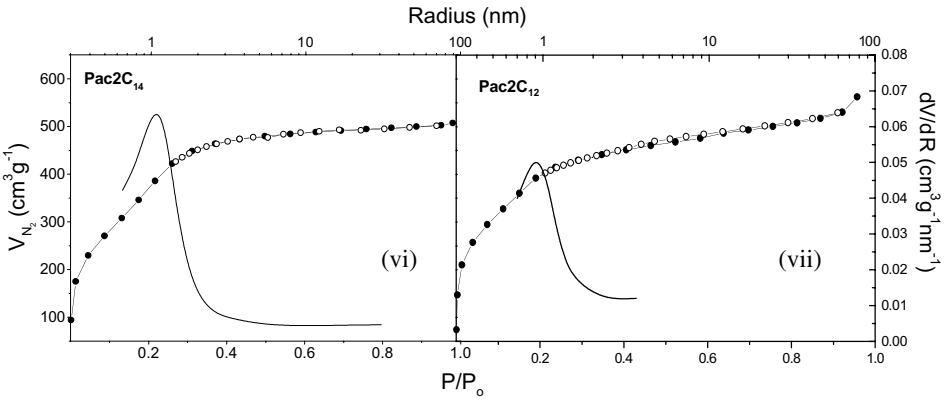


Fig. 5 (*continued*)

These results support the findings by XRD and TEM that the samples obtained with Pac of lower MW, or without Na, are better organized. The cubic materials $Pa2C_{14}$ and $Pac2C_{12}$ exhibit not as steep condensation steps as the hexagonally structured materials owing probably to their special structural characteristics and smaller pores.

## 4. Discussion

The structural characteristics of the materials prepared are summarized in Table 1. The pore volume, the Horvath–Kawazoe (HK) pore diameter and the cell parameter in the Pac*X*$C_{16}$ series is controlled by the polyelectrolyte and increases with increasing polyacrylic acid chain length. For the Pac15(Na)$C_{16}$ calcined sample we observe a small decrease of pore volume and cell parameter compared with $Pac2C_{16}$ sample. This is probably due to the use of the sodium salt of polyacrylic acid and the remaining sodium cations, which during calcination can be the cause of serious framework defects.

The SBA-1 phase is stabilized by shorter chain surfactants. Both the surfactant and the polyelectrolyte appear to affect the cell parameter $a_0$ and pore diameter (Table 1). The latter increases from 1.8 to 2.2 nm with increasing the surfactant chain length but keeping the polyacrylic acid chain length constant ($Pac2C_{12}$ and $Pac2C_{14}$). The same effect is observed for the uncalcined samples, where increasing the polyelectrolyte chain length and keeping the surfactant chain length constant (Pac15(Na)$C_{14}$ and $Pac2C_{14}$) leads to an increase of the $a_0$ parameter from 7.4 to 8.4 nm. The thermal stability of the cubic phase is negatively affected by polyelectrolyte chain length as it was not possible to generate highly thermally stable materials. However, the use of the sodium salt of Pac and the remaining sodium cations on the framework cause deterioration in the order of structures (Fig. 4).

The polyelectrolyte apart from controlling the pore openings controls also the size of the particles. The SEM micrographs (Fig. 2) reveal a decrease in particle size of the corresponding materials from about 1 μm for $Pac2C_{16}$ to almost 100 nm for $Pac450C_{16}$. Moreover the larger uncalcined particles (inset of Fig. 2a) are made up like flakes with hexagonally shaped ($Pac2C_{16}$) morphologies, whilst smaller particles show no such tendency. This can be explained if we accept that smaller size of primary micelles result in bigger crystal-like particles, while larger primary particles favor the development of macroscopically smaller particles. This effect can be attributed to the more effective aggregation of smaller and better-organized micelles (i.e. $Pac2C_{16}$) towards larger secondary particles. On the contrary, larger and less organized

micelles (i.e. Pac450$C_{16}$) cannot be easily developed towards big, ordered aggregations/crystallites.

## 5. Mechanism of development of mesostructures

The formation of polyacrylic acid–$C_n$TAB complexes takes place according to the following reaction:

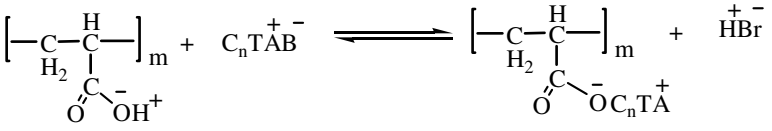

(1)

where $m$—the degree of polymerization of acrylic acid. It is clear from the above reaction that in strongly acidic conditions the equilibrium shifts to the left and not appreciable amount of Pac–$C_n$TA is formed. But as the pH increases and the equilibrium moves to the right, gradually larger amount of Pac–$C_n$TA *organic* complex separates from the solution. A good insight into the evolution of the obtained organic mesophase (Pac–$C_n$TA) can be obtained by probing the conductivity $C$ of the solution against the increase of pH. Such conductivity experiments in the form $C = f(\mathrm{pH})$ are shown in Fig. 6. Those graphs were obtained as described in the experimental part and under the same conditions of the synthesis protocol.

In Fig. 6, the upper part shows the titration curves $C = f(\mathrm{pH})$ for the three systems which contain polyacrylic acid with $\mathrm{MW} = 2000\ \mathrm{g\,mol^{-1}}$, (Pac2) namely, Pac2/W, Pac2/$C_{16}$TAB/W and Pac2/$C_{16}$TAB/TEOS/W (W stands for water). These three curves have similar shapes and bear the blueprint of the titration curve of Pac2/W. This is a typical titration profile between the weak polyacrylic acid and a weak base ($NH_3$). This curve exhibits two points of zero gradient, at $\mathrm{pH} \approx 3.3$ and $\mathrm{pH} \approx 7.6$, corresponding to two isodynamic points (I), related to the neutralization of the added HCl acid and (II) as described by the equilibrium reaction shown on the top of this figure.

The other two curves, corresponding to Pac2/$C_{16}$TAB/W and Pac2/$C_{16}$TAB/TEOS/W systems, show similar trends in general with some important differentiation we shall discuss next.

In the lower part of Fig. 6, the corresponding titration curves for TEOS/W and TEOS/$C_{16}$TAB/W are shown. Those two curves appear totally different as compared to the ones corresponding to solutions containing Pac. Now, an important point we should mention is that the successive points in those curves correspond to addition of equal amount of $NH_3$ 0.1 M. It is clear, therefore, that the addition of equal amounts of base does not influence the pH equally, but in some cases increases it more, while in others much less. Such is, for example, the case between the titration curves for the TEOS/$C_{16}$TAB/W and the TEOS/W systems: In the first case at $\mathrm{pH} \approx 4.8$, right after the pH range 4.3–4.8, where the gradient is zero, successive addition of base does not increase the pH, as it does for the TEOS/W system. Additionally, at this $\mathrm{pH} \approx 4.8$, the first appearance of colloidal particles takes place for the TEOS/$C_{16}$TAB/W system and conductivity increases in a linear manner with pH. The corresponding range of zero gradient for the TEOS/W system lies at $\mathrm{pH} = 4.7$–5.4, while right after $\mathrm{pH} \approx 5.4$ particle formation takes place and conductivity increases in a linear manner with pH also. So it becomes clear that the linear part of those two curves is directly related to the condensation and polymerization of silica. It is worthnoticing, as mentioned above, that the gradient of the line of TEOS/$C_{16}$TAB/W system (right hand end of the curve) is steeper than the corre-

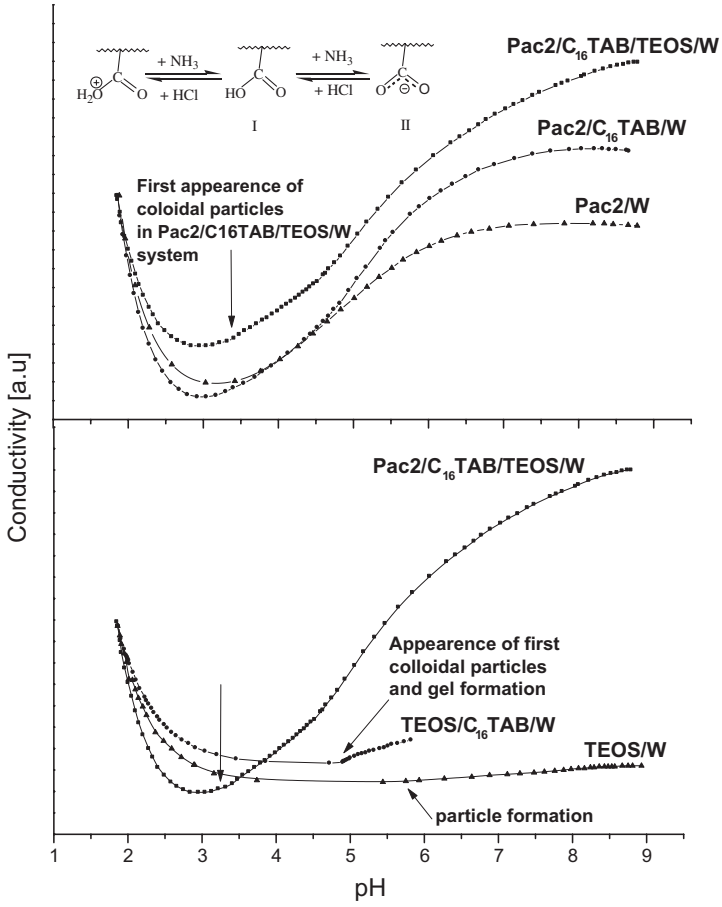


Fig. 6. Variation of conductivity of the indicated solutions as a function of pH ($NH_3$ addition). The successive points in each titration curve correspond to equal successive additions of $NH_3$ solution. Nevertheless, the conductivity is affected in a different way by the equal addition of $NH_3$ along each titration.

sponding one for the TEOS/W system, implying a higher rate of silica polymerization reaction. The acceleration of silica polymerization reaction is a characteristic feature of the cooperative self-assembly in hybrid organic/inorganic systems like TEOS/$C_{16}$TAB/W as widely accepted [17]. Note, however, that no ordered material is generated by the system TEOS/$C_{16}$TAB/W under the synthesis conditions, as revealed by the $N_2$ adsorption–disorption isotherms, shown in Fig. 5 (middle). In this sample, a bimodal pore size distribution is apparent with a very small and broad condensation step in the lower region of relative pressure, indicating disordered worm-like structure. This result is also in agreement with low angle XRD measurement of that sample, which reveals the inexistence of low angle peaks (not shown).The secondary porous network evident in the higher region of relative pressure, is probably built up as a result of an agglomerating process of the primary particles.

So, the main conclusion that we should keep in mind from these conductivity experiments and which will be used in the following discussion, is that the initiation of a phase separation for the TEOS/$C_{16}$TAB/W system takes place at pH $\approx$ 4.8, while complexion of the negatively charged silica oligomers with surfactant can be assumed to occur

in pH range 2–3 (isoelectric and point of zero charge of silica) [18] up to 4.8.

Let us now go back and discuss in more detail the relevant titration curves in the upper part of Fig. 6.

If we compare the titration curve for the system Pac2/$C_{16}$TAB/W with that for Pac2/W, we observe that in the first case the gradient d*C*/dpH is steeper, in the negative slope of the curve. This means that reaction (1), occurring in Pac2/$C_{16}$TAB/W is faster—and preferable—to reaction (2), occurring in Pac2/W.

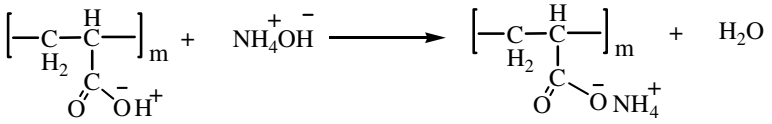

(2)

In other words the cationic surfactant is preferably complexed with Pac leading to the separation of the highly ordered organic complex according to reaction (1) and cannot contribute to conductivity anymore. Besides the first isodynamic point of Pac2/$C_{16}$TAB/W system is shifted to lower values of pH ≈ 2.8, instead of 3.3 of Pac2/W system-influenced possibly by the Pac–$C_{16}$TAB complexion and the resulting phase separation.

The main conclusion, derived by the comparison of the two curves, that we should have in mind for the following elaboration, is that Pac2–$C_{16}$TAB complexion, which leads to the formation of a liquid crystalline (organic) mesophase [11], takes place in the pH range ≈2–2.8, before occurrence of phase separation.

Addition of TEOS (Pac2/$C_{16}$TAB/TEOS/W) results in higher conductivity values because of its hydrolized silicate products (dimers, trimers, tetramers and cyclic compounds), which would gradually carry a higher negative charge density, as pH is increased, would lead to increased conductivity values. The first isoelectric point lies at pH ≈ 2.8—exactly the same as for the system Pac2/$C_{16}$TAB/W. Immediately after this and at pH ≈ 3.3 the first appearance of colloidal particles is clearly seen by naked eye.

A reasonable question posed at this point is whether this precipitated solid is just the organic complex (which separates at pH ≈ 2.8–3.3 as shown in the upper part of Fig. 6) or a hybrid organic/inorganic composite material. The last case strongly indicates that Pac2–$C_{16}$TAB organic nanoassembly causes immediate silica condensation and polymerization on this preformed matrix in a cooperative self-assembling process. Note, that as mentioned above the initiation of a phase

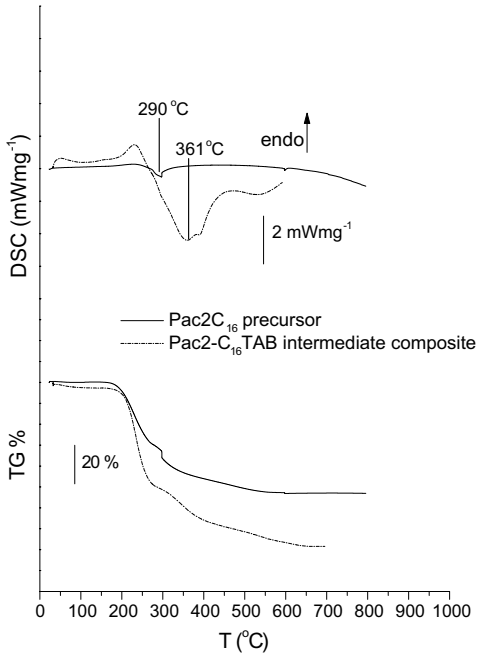


Fig. 7. Typical TG–DSC signals of the sample isolated at the intermediate pH ≈ 3.3 (Pac2–$C_{16}$TAB intermediate composite) and at the final pH ≈ 5.5 (Pac2$C_{16}$ precursor).

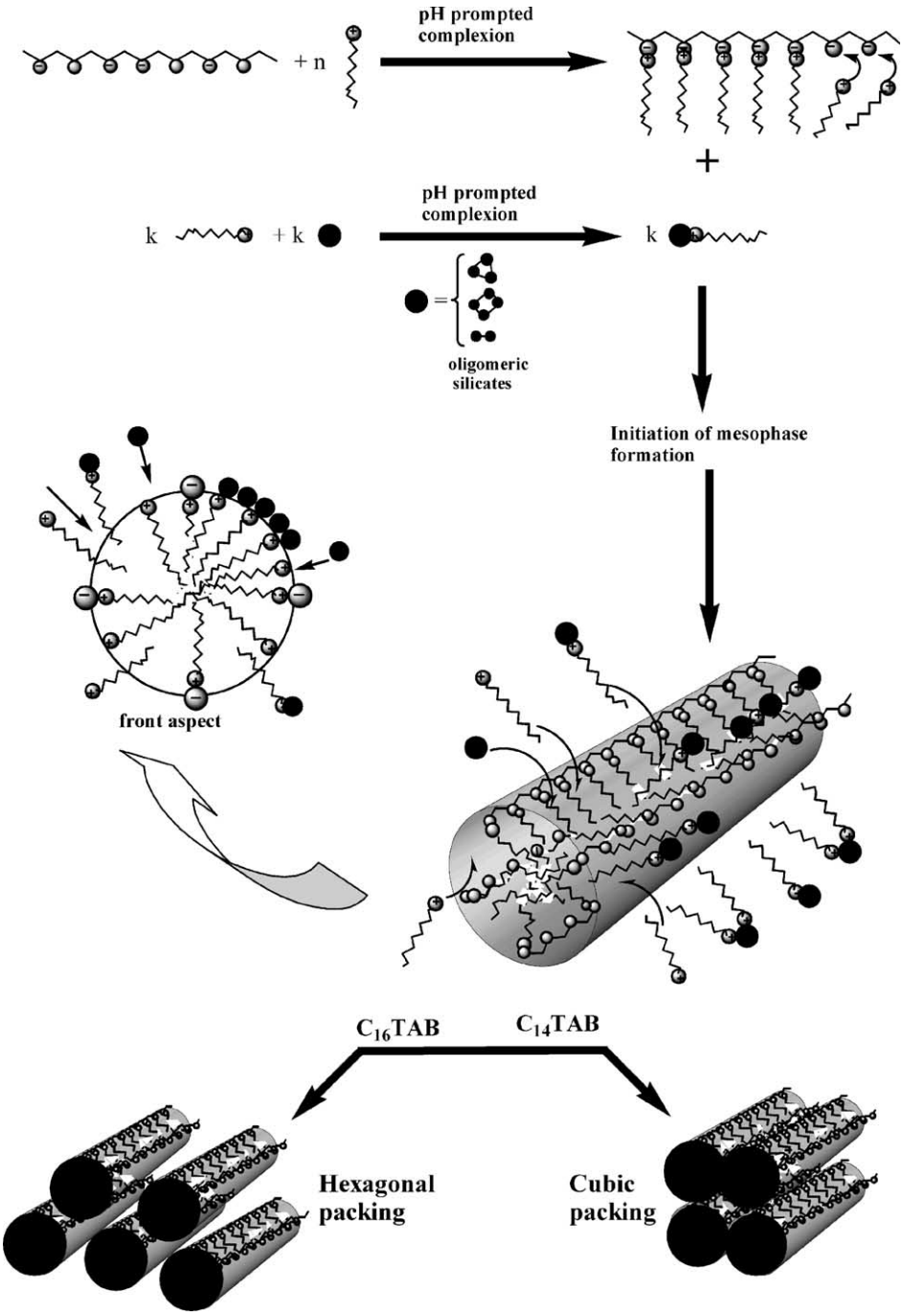


Fig. 8. A schematic illustration of the self-assembly. The pH-prompted polyelectrolyte–surfactant complexion according to a zipper mechanism, which leads to topologically fixed assemblies of rod-like micelles, is shown. At the same time the existing uncomplexed or complexed with surfactant oligomeric silicate species, are attracted by the micelle and condense on the matrix. Depending on the surfactant chain length, cubic or hexagonal packing is preferred. The black spheres correspond to silicate species.

separation for the TEOS/$C_{16}$TAB/W system takes place at pH $\approx$ 4.8.

A first strong indication that this is actually the case is provided by thermogravimetric analysis shown in Fig. 7 as well as EDS analysis of the calcined intermediate, which reveals conclusively that the composite contains polymerized silica.

In this figure the TG and DSC signals of an intermediate sample isolated at pH $\approx$ 3.3 is compared with the final sample. The intermediate sample indeed contains $\approx$21% of inorganic phase ($\approx$79% weight loss) compared to $\approx$47% of the final material ($\approx$53% weight loss). The corresponding DSC shows an exothermic signal for the two samples due to burning of CTAB. However, the signal of the intermediate is stronger, indicating higher percent of organic phase and also shifted to higher temperature, indicating a more strongly bind nanocomposite [19].

The above results are in accordance with the indications provided by the $C = f(\mathrm{pH})$ curve of Pac2/$C_{16}$TAB/TEOS/W. The linear part in this curve between $3.3 < \mathrm{pH} < 4.6$ is obviously induced by the condensation and polymerization reactions of silica as observed in TEOS/$C_{16}$TAB/W between $4.8 < \mathrm{pH} < 5.8$ and TEOS/W system between $5.4 < \mathrm{pH} < 8.8$ and has even higher gradient than the corresponding line of TEOS/$C_{16}$TAB/W system implying even higher reaction rates resulting from a stronger cooperative self-assembling.

Taking into consideration the main points of the previous discussion, we can propose a pathway for the self-assembly, as depicted in Fig. 8. This includes initially the formation of Pac*X*–$C_n$TAB mesophase form pH 1.5 up to pH $\approx$ 3.2–3.3. This structure provides a starting preformed (as indicated by conductivity experiments above) scaffold and a pole of attraction for the silicate species complexed to the $C_n$TAB.

These last entities—$C_nTA^+$–$SiO_x^-$—are thus properly coordinated on the central matrix Pac*X*–$C_n$TAB. As a result an increase in the concentration of silicate species is observed on the interface of (Pac*X*–$C_n$TA)//($C_n$TA–$SiO_x$) assembly. Finally, the increase of the pH leads to a gradual increase in condensation and polymerization rates (compared to TEOS/$C_{16}$TAB/W system), resulting in mesostructures and mesoporous materials whose order is controlled by both the surfactant chain length ($C_{16}$TAB, $C_{14}$TAB, $C_{12}$TAB) and/or the polyelectrolyte chain/backbone. The polyelectrolyte is a necessary structural component under the synthesis protocol as established above, while surfactant is the phase determining species as $C_{16}$TAB leads to hexagonal, while $C_{14}$TAB and $C_{12}$TAB. That has probably to do with change of curvature. $C_{14}$TAB and even more $C_{12}$TAB induces higher curvature which favors the cubic phase.

Some more considerations on the mechanism have to be made. At this point we cannot support the formation of an organized preformed matrix as literature on highly ordered polyelectrolyte–surfactant complexes refers to almost neutral conditions where all the functional groups of the polyelectrolyte are ionized and complexed to the surfactant. However, at pH 2–3 we do not know if Pac–$C_n$TAB complex has formed an organized phase and probably this is not the case. That preformed matrix at the early steps of its formation (pH 1.5 to 2–3) acts as a pole of attraction for the complexed with surfactant silicates at pH 2–3. At this pH slightly above the isoelectric point of silica we have no reason to exclude the existence of silica-surfactant species. This is the case we refer to in this work. Below pH 2–3 $^{29}$Si NMR spectroscopy could give some clues to an even more detailed mechanism. Finally, the degree which condensation and polymerization of silica on the preformed matrix contributes to the final structure is not known. Further research is under way in order to clarify these points which will provide more insight to the evolution of the mesophase formation.

## 6. Conclusions

This work explores a new pathway of self-organization leading to highly ordered hexagonal MCM-41 and/or cubic SBA-1 type mesostructured and mesoporous silica, by employing polyacrylic acid–$C_n$TAB preformed nanoassemblies as a scaffold coated eventually by the inorganic silicate phase. The surfactant species is the phase determining agent. Hexagonal structures are obtained

with the use of $C_{16}$TAB, while cubic ones with $C_{14}$TAB and $C_{12}$TAB, independently of the polyelectrolyte chain length. The mesoporosity, the cell size as well as the size of particles of the materials are influenced by both the polyelectrolyte and the surfactant. The system is differentiated from the existing ones by the pre-formation of the alkyl matrix Pac–$C_n$TAB followed by coating of this matrix by the $SiO_2$ inorganic phase. Finally, a very important implication of this work is that it makes possible the synthesis of the SBA-1 phase under almost neutral conditions.

## Acknowledgements

We thank the European Union for funding this work under the INORGPORE program (project G5RD-CT-2000-00317). We also acknowledge the SEM and XRD units of the Ring of Laboratory Units and Centers of the University of Ioannina.

## References

[1] J.S. Beck, J.C. Vartuli, W.J. Roth, M.E. Leonowicz, C.T. Kresge, K.D. Schmitt, C.T.-W. Chu, D.H. Olson, E.W. Sheppard, S.B. McCullen, J.B. Higgins, J.L. Schlenker, J. Am. Chem. Soc. 114 (1992) 10834.

[2] (a) Q. Huo, D.I. Margolese, U. Ciesla, P. Feng, T.E. Gier, P. Sieger, R. Leon, P.M. Petrof, F. Schuth, G.D. Stucky, Nature 368 (1994) 317;
(b) Q. Huo, D.I. Margolese, U. Ciesla, D.G. Demuth, P. Feng, T.E. Gier, P. Sieger, A. Firouzi, B.F. Chmelka, F. Schuth, G.D. Stucky, Chem. Mater. 6 (1996) 1176.

[3] D. Zhao, Q. Huo, J. Feng, B.F. Chmelka, G.D. Stucky, J. Am. Chem. Soc. 120 (1998) 6024.

[4] G.C. Goltner, S. Henke, M.C. Weissenberger, M. Antonietty, Angew. Chem. 10 (1998) 633.

[5] P.T. Tanev, T.J. Pinnavaia, Science 267 (1995) 865.

[6] X. He, D. Antonelli, Angew. Chem. Int. Ed. Engl. 41 (2001) 214.

[7] A. Stein, B.J. Melde, R.C. Schroden, Adv. Mater. 12 (2000) 1403.

[8] R. Ryoo, S.H. Joo, M. Kruck, M. Jaroniec, Adv. Mater. 13 (2001) 677.

[9] (a) S. Oliver, N. Coombs, A. Kuperman, A. Lough, G.A. Ozin, Nature 378 (1995) 47;
(b) G.A. Ozin, A. Kuperman, D. Khushalani, N. Coombs, K. Tanaka, Adv. Mater. 7 (1995) 842.

[10] (a) D. Walsh, S. Mann, Nature 377 (1995) 320;
(b) D. Walsh, J.D. Hopwood, S. Mann, Science 264 (1994) 1576.

[11] M. Antonietti, J. Conrad, Angew. Chem. Int. Ed. Engl. 33 (1994) 869.

[12] M. Antonietti, J. Conrad, A. Thuneman, Macromolecules 27 (1994) 6007.

[13] M. Antonietty, G.C. Goltner, Angew. Chem. Int. Ed. Engl. 36 (1997) 910.

[14] K. Hayagawa, J.P. Santere, J.C.T. Kwak, Macromolecules 16 (1983) 1642.

[15] (a) P. Flory, Principles of Polymer Chemistry, Cornell University Press, 1953;
(b) A.W. Adamson, A.P. Gast, Physical Chemistry of Surfaces, J. Willey-Interscience, New York, 1997.

[16] S. Che, Y. Sakamoto, O. Terasaki, T. Tatsumi, Chem. Mater. 13 (2001) 2237.

[17] A. Monnier, F. Schuth, Q. Huo, D. Kumar, D.I. Margolese, R.S. Maxwell, G.D. Stucky, M. Krishnamurty, P. Petroff, A. Firouzi, M. Janicke, B.F. Chmelka, Science 261 (1993) 1299.

[18] C.J. Brinker, G.W. Scherer, Sol–Gel Science, Academic Press, Inc., New York, 1990, p. 103, 124, 169.

[19] H. Kosslick, G. Lischke, H. Landmesser, B. Parlitz, W. Storeka, R. Fricke, J. Catal. 176 (1998) 102.